Molecular Packing in Electroclinic Liquid Crystal Elastomer Films

Christopher M. Spillmann,[†] John H. Konnert,*[,‡] Jeffrey R. Deschamps,[‡] Jawad Naciri,[†] and Banahalli R. Ratna[†]

Center for Bio/Molecular Science and Engineering and Laboratory for the Structure of Matter, Naval Research Laboratory, 4555 Overlook Avenue SW, Washington, D.C. 20375

Received May 16, 2008. Revised Manuscript Received July 28, 2008

The structure and molecular packing of an electroclinic liquid crystal elastomer (ELCE) is examined using X-ray diffraction in an unstressed state, under mechanical load, and in the presence of electric fields of varying strength and opposing polarity. A fully three-dimensional pattern of the unstressed elastomer is constructed revealing a detailed look into the molecular packing. Several expected features have been observed in the elastomer film, including well-ordered smectic layering, chevron formation under increasing mechanical load, and molecular reorientation accompanied by layer contraction in the presence of an electric field. Additional intralayer rearrangements related to the molecular switching in the presence of an electric field have also been observed. A model based on periodic pair distribution functions is presented to explain the X-ray scattering observations under each of the tested conditions, starting with the observation that layer-related diffraction bands cannot simply be indexed as higher-order reflections. The model provides key insights toward a complete understanding of the molecular packing and origins of the electroclinic response in an elastomeric system.

Introduction

One approach toward the development of a soft linear actuator is the incorporation of liquid crystal molecules that exhibit a chiral smectic A (SmA*) phase into an elastomer network. Garoff and Meyer first described a phenomenon known as the electroclinic effect, wherein an electric field is applied to chiral liquid crystal monomers along the layer plane and the molecular transverse dipole couples to the electric field.[1,2] The result is a molecular tilt that varies continuously with e-field strength and is constrained in a plane perpendicular to a plane defined by the mesogenic director and the transverse component of the permanent molecular dipole.

By incorporating electroclinic molecules into an elastomeric network, an applied electric field can be used to induce reversible shape change of a liquid crystal elastomer (LCE). The underlying mechanism of the elastomer shape change is a reorientation, i.e., tilt, of the electroclinic liquid crystal molecule due to realignment of the permanent molecular dipole in the presence of an electric field. The degree of molecular tilt and alignment of the molecular dipole depend upon the strength and polarity of the applied field, respectively. Tight coupling of the molecular reorientation to the polymer network causes a macroscopic contraction along the layer normal and a shearing extension in the direction of the smectic layers and orthogonal to the direction of the electric field.[3] The layer contraction may be understood from a simple two-dimensional geometric consideration where the change in the smectic layer spacing, Δl, is proportional to the cosine of the molecular tilt. The magnitude of the contraction is equal when the field strength is held constant but the polarity reversed. Likewise, the extent of the shear is independent of the e-field polarity while the direction of the shear is reversed.

There are several aspects of the molecular packing and orientation that may change upon actuation of an electroclinic elastomer. From two-dimensional geometric arguments, it is obvious that molecular tilting will result in layer contraction with an additional shear component parallel to the layers, but the details of how this occurs on a molecular level in an electrically actuated liquid crystal elastomer are largely unknown and unexplored. A fundamental understanding of the changes in molecular packing and reorientation when an electric field is applied would elucidate the relation between molecular order and actuation.

The study of liquid crystalline polymers and elastomers via X-ray scattering has long confirmed the presence of significant anisotropy locked into the underlying polymer network.[4−7] The experimental study and theoretical analysis of a subset of these materials, i.e. elastomeric networks exhibiting smectic order, has attracted much interest on the basis of the formation of free-standing smectic elastomers.[3,5,8−15]

* Corresponding author. E-mail: john.konnert@nrl.navy.mil. Phone: (202) 767-3276. Fax: (202) 767-6874.

[†] Center for Bio/Molecular Science and Engineering, Naval Research Laboratory.

[‡] Laboratory for the Structure of Matter, Naval Research Laboratory.

(1) Garoff, S.; Meyer, R. B. *Phys. Rev. Lett.* **1977**, *38*, 848.
(2) Garoff, S.; Meyer, R. B. *Phys. Rev. A* **1979**, *19*, 338.
(3) Spillmann, C. M.; Ratna, B. R.; Naciri, J. *Appl. Phys. Lett.* **2007**, *90*, 021911.
(4) Azaroff, L. V. *Mol. Cryst. Liq. Cryst.* **1987**, *145*, 31.
(5) Hiraoka, K.; Sagano, W.; Nose, T.; Finkelmann, H. *Macromolecules* **2005**, *38*, 7352.
(6) Kostromin, S. G.; Sinitzyn, V. V.; Talroze, R. V.; Shibaev, V. P.; Plate, N. A. *Makromol. Chem.−Rapid Commun.* **1982**, *3*, 809.
(7) Weilepp, J.; Brand, H. R. *Europhys. Lett.* **1996**, *34*, 495.
(8) Adams, J. M.; Warner, M. *Phys. Rev. E* **2005**, *72*, 011703.
(9) Adams, J. M.; Warner, M. *Phys. Rev. E* **2005**, *71*, 021708.

10.1021/cm801335j CCC: $40.75
Published on Web 09/23/2008

Of particular interest has been the molecular changes that occur in smectic elastomers when under mechanical load (tensile and shearing forces) and also subjecting these films to changes in temperature to explore the thermal transition of a smectic elastomer between the chiral SmC and A phases.[5] X-ray scattering studies on such a system revealed a nonlinear relationship between the tilt angle resulting from the elastomer film shearing and the molecular tilt angle. It was suggested that the discrepancy between these values may have been a consequence of the cross-linking topology, an effect that has been suggested previously.[16,17] Analogous to the SmA-C thermal transition is the electrically induced response in SmA* elastomers. Early reports proved the viability of such systems, but relied upon analysis of submicron thick samples via interferometric techniques and allowed for limited molecular packing analysis with X-ray diffraction.[11−13]

A recent breakthrough in the field of liquid crystal elastomers led to the creation of a thick, free-standing electroclinic elastomer with a measurable macroscopic contraction and shearing in response to an electric field.[3] The macroscopic response was correlated to the expected contraction and shear based on the tilt angle measurements of the molecular core using electro-optic techniques. In this report, we provide the first detailed X-ray diffraction study on the molecular packing and orientation of a SmA* elastomer in an unstressed state and subjected to either mechanical loading or application of an electric field. The diffraction patterns could not be explained simply by indexing the diffraction bands as higher order reflections of one another. Therefore, a model based on periodic pair distribution functions (PPDFs) is proposed to explain these observations and provide a fundamental understanding of the molecular packing and reorientation in an electroclinic elastomer.

Experimental Section

Preparation of Elastomer Films. The electroclinic elastomer consists of a 70/30 weight % (eutectic) mixture of chiral mesogenic monomers ACN115 and ACBN115, respectively, and 5 mol % of a cross-linker (DACP11). The molecular structures of the materials are shown in Figure 1a. The procedure of creating the free-standing elastomer films has been described elsewhere.[3] In brief, the mixture is filled into a glass cell of known thickness and aligned by slow cooling and application of an electric-field (±6V/μm, 0.5 Hz, square wave). The glass is first coated with rubbed polyimide and then a second sacrificial layer of rubbed polyvinyl alcohol (PVA). Once the mixture has been aligned, the e-field is removed and the sample is immediately photopolymerized under UV light. The PVA is then dissolved in water allowing the elastomer to be extracted from the glass cell. The thickness of the film (~60 μm) was measured with a micrometer and the liquid crystal alignment was confirmed with polarized light microscopy.

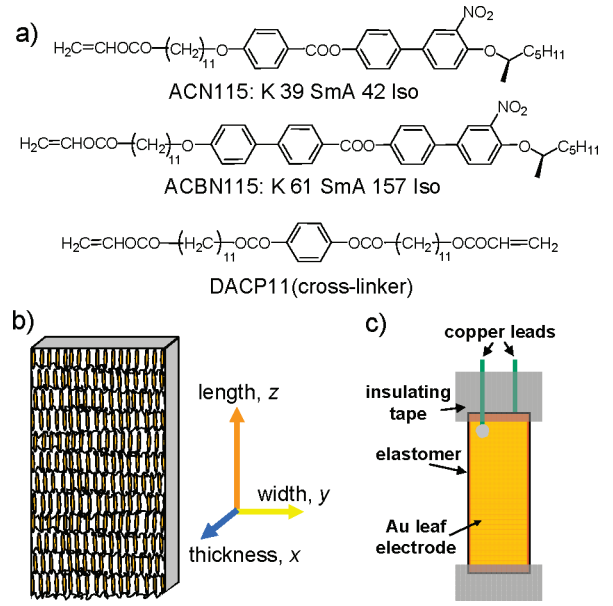

Figure 1. Electroclinic effect of an elastomer film. (a) Chemical structures of electroclinic mesogens and cross-linker. (b) Schematic representation of elastomer with coordinate system definitions. (c) Experimental setup to measure diffraction pattern changes of the elastomer with either an applied electrical field or mechanical loading.

X-ray Diffraction Studies. Diffraction data was collected using Cu Kα radiation and a Bruker SMART 6000 CCD on an FR-591 generator equipped with Göbel optics. The configuration allows data collection corresponding to an upper limit *d*-spacing of ~55 Å. Samples for 2D X-ray diffraction studies were prepared by cutting pieces of the electroclinic LCE film either along the *z* or *y* axis and mounting the films so that the X-ray beam was aligned with the *x* axis (see Figure 1b for axis orientations).

A full three-dimensional diffraction pattern of the unstressed elastomer was collected by mounting a small piece of the film (~5 × 5 × 0.05 mm^3) on a plastic grid (MiTeGen LLC, Ithaca, NY) with high viscosity microscope oil (Paratone-N, Hampton Research, Laguna Niguel, CA). A ϕ scan of the sample was collected in 1° increments and the resultant diffraction patterns were assembled into a 3D image using in-house software. Each 2D pattern was obtained as a 512 × 512 array of pixels. The three-dimensional pattern is assembled and stored as a 512 × 512 × 512 array of voxels and may be sampled and displayed in any desired manner.

Mechanical Loading. A schematic of the experimental setup for mechanical loading is shown in Figure 1c (minus the electrodes and copper leads). Insulation tape placed on the top and bottom of the sample was added to maintain an even load distribution over the surface of the film and to keep the surface of the film normal to the X-ray beam. An initial diffraction pattern was captured prior to loading the film. Subsequently, a binder clip (providing a load of 12 mN) was added to the lower piece of insulation tape, following by the incremental addition of 6mN of tensile stress to the film. Diffraction images were captured after each weight was added until a maximum load of 84 mN (~310 kPa) was applied. The sample did not yield under this maximum applied stress.

Electric-Field Application. For experiments requiring the application of an electric-field, a conformal electrode of gold leaf was applied to both sides of the sample surface. The electrodes were thin enough to allow collection of the sample's diffraction pattern yet thick and compliant enough to tolerate actuation of the sample

(10) Adams, J. M.; Warner, M. *Phys. Rev. E* **2006**, *73*, 031706.
(11) Kohler, R.; Stannarius, R.; Tolksdorf, C.; Zentel, R. *Appl. Phys. A: Mater. Sci. Process.* **2005**, *80*, 381.
(12) Lehmann, W.; Skupin, H.; Tolksdorf, C.; Gebhard, E.; Zentel, R.; Kruger, P.; Losche, M.; Kremer, F. *Nature* **2001**, *410*, 447.
(13) Stannarius, R.; Kohler, R.; Dietrich, U.; Losche, M.; Tolksdorf, C.; Zentel, R. *Phys. Rev. E* **2002**, *65*, 041707.
(14) Stenull, O.; Lubensky, T. C. *Phys. Rev. Lett.* **2005**, *94*, 018304.
(15) Nishikawa, E.; Finkelmann, H. *Macromol. Chem. Phys.* **1999**, *200*, 312.
(16) Gebhard, E.; Zentel, R. *Macromol. Chem. Phys.* **2000**, *201*, 902.
(17) Gebhard, E.; Zentel, R. *Macromol. Chem. Phys.* **2000**, *201*, 911.

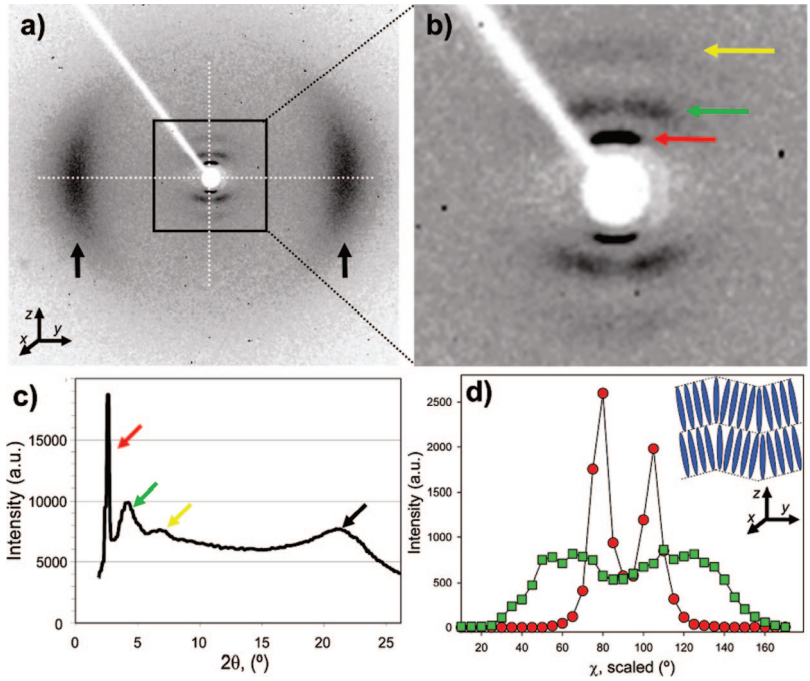

Figure 2. Diffraction pattern of an unstressed ELCE film mounted with the z axis aligned vertically. (a) Entire diffraction image showing 4.3Å bands (black arrows). (b) Zoomed in view of three layer-related bands at 38, 24, and 14 Å labeled with a red, green, and yellow arrow, respectively. (c) Scattering intensity profile of unstressed elastomer as a function of solid cone angle, 2θ. (d) Scattering intensity plotted as a function of χ highlighting the splitting of the 38 Å (red) and 24 Å (green) bands. (Intensity of 24 Å feature has been amplified 5×.) Inset: Molecular scheme depicting chevron-like domains related to the splitting of the 38 Å band.

upon field application. (Diffraction from the gold electrodes was also used to calibrate the sample to detector distance.) As shown in Figure 1c, two thin copper leads were placed in contact on either sample surface. The leads were in-line with a voltage amplifier and function generator used for the application dc fields. A nickel−chromium heating element below the sample was used to maintain the temperature at 40 ± 5 °C. Samples were suspended and aligned with the thickness (x axis) parallel to the X-ray beam. With the electrodes confined to the y, z plane, the applied electric field was directed along the x-axis (Figure 1b). In response to the field, the permanent electric dipoles (nitro groups shown in Figure 1a) of the electroclinic molecules rotate to align with the field along the x-axis in a polarity dependent manner. The corresponding molecular tilt and changes in layer-related information were indicated by the diffraction image.

To capture diffraction images of the samples under the influence of an e-field, a dc voltage was applied for at least 2 min to ensure the equilibrium state of the elastomer. Following this wait period, two successive frames were recorded at each voltage with an exposure time of 120s. The voltage was ramped in 200 V increments from 0 to 1600 V (27 V/μm) and diffraction images were captured under both positive and negative polarity at each field strength.

Results

Unstressed Elastomer. An X-ray diffraction image of an unstressed ELCE film mounted with the X-ray beam aligned with the x axis is shown in Figure 2. After correcting for the sample to detector distance, the spacings of four identifiable scattering bands are determined by integrating around χ as a function of the solid cone angle, 2θ (Figure 2c). The broadband on the horizontal axis located at 4.3 Å corresponds to the average intermolecular spacing between the liquid crystal mesogens (Figure 2a, black arrows) and is approximately orthogonal to the three small angle features. The bands on the vertical axis, which correspond to smectic layer spacing information, are located at 38 and 24 Å with a faint third band at 14 Å (Figure 2b, red, orange, yellow arrows, respectively). The peak intensity and corresponding width of the 38Å band indicates a periodicity extending over several hundred angstroms both along the film length and width (z and y axes). Put another way, the order correlation along z persists in diminished manner over more than 30 layers. Given the length of the liquid crystal molecular components of the elastomer (42−44 Å), the 38Å band is associated with the average smectic layer spacing of the sample. The 24 and 14 Å peak widths are broader indicating a short-range correlation order extending over less than 100 Å and, thus, only extending over several smectic layers.

There are two additional observations of the smectic layer bands in the unstressed elastomer. First, the diffraction bands associated with the smectic layering cannot be indexed simply as higher order reflections of the primary. Additional bands are expected to be present in order to confidently assign the d-spacings related to the smectic layering as higher order reflections and, therefore, indicate that the 24 and 14 Å bands may be related to intrasmectic layer features of the elastomer combined with scattering contributions from the smectic layer itself.

The second observation is a sharp and weak splitting of the 38Å and the 24Å bands about χ, respectively (see panels b and d in Figure 2). The splitting indicates that on a molecular level the elastomer sample is not uniaxial but contains two preferred chevron-like domains, i.e., smectic layer domains rotated with respect to one another along the y-axis (see Figure 2d, inset). Assuming the 38 Å band represents the primary smectic layer spacing within the

elastomer, the rotated layer domains deviate ~15° from a plane orthogonal to the direction of the intermolecular packing and can be thought of as small undulations along smectic layers in the *y* direction. Further analysis shows the degree of χ splitting for the 24 Å peak (~26°) as being significantly greater than the χ splitting of the 38 Å peak (Figure 2d). Equal χ splitting of the 38 and 24 Å peaks would point toward only two preferred domains within the elastomer, but this additional information indicates that the elastomer packing is more complex. The increased χ splitting of the 24 Å band reveals the presence of an intralayer feature within the elastomer with an average deviation from a plane orthogonal to the direction of the intermolecular packing that is greater than just the chevron-like tilt resulting in the split of the 38 Å band.

All two-dimensional diffraction patterns represent a single curved surface in the full three-dimensional reciprocal space diffraction pattern of the elastomer. Therefore, a three-dimensional diffraction pattern was assembled from two-dimensional patterns obtained in 180 different orientations with the unstressed material, as shown in Figure 3. The 38 and 24 Å features have been expanded by a factor of 2 relative to the outer 4.3 Å feature. (The weak 14 Å feature has been intentionally excluded in the figure to unmask the 24 and 38 Å information.) To the best of our knowledge, this is the first time such a detailed observation has been made of a smectic elastomer and provides a unique look into the molecular order within the confines of the elastomeric network.

As shown in Figure 3a, the 3D diffraction pattern of the film reveals cylindrical symmetry about the director for the 4.3 Å information. The apparent minima along the *x*-axis in panels a and d in Figure 3 are missing data, an artifact of the diffraction data being collected by rotating the sample about a single axis. The 24 Å scattering is saucer-shaped, while the 38 Å scattering looks like two three-dimensional ellipsoids stacked next to one another (Figure 3b). The obvious splitting observed in the 38 Å feature highlights the presence of two preferred chevron-like domains for the smectic layers (Figure 3b, green arrows). The less prominent splitting of the 24 Å feature is also present in the 3D data (Figure 3b, blue arrow), once again indicating an accompanying intralayer ordering with a greater angular deviation from the *z*-axis. (The 14 Å feature is also present, but is too weak to extract any meaningful information beyond its approximate position along 2θ.) When the 3D data is viewed along the sample width (*y* axis), there is no observable splitting of the smectic layer features (Figure 3c) despite a prominent angular spread that peaks in the *y*, *z* plane (parallel to the elastomer surface). For the 38 Å band, the full width of the angular spread at half-height is found to be ~45°. It is possible that some of this elongation could be due to limited thickness of the ordered regions.

To further describe the layer-relevant scattering from the 3D data, one can imagine observing the topology of a smectic layer within the elastomer. Along the width of the film (*y* axis), there are two preferred domains deviating ±15° away from the *z*-axis in the *y*, *z* plane. The two preferred domains would be randomly distributed over the smectic layer. On the other hand, the topology through the thickness of the film (*x* axis) does not consist of two preferred domains, but rather a random distribution of deviations of 45° at full width, half-height in the *x*, *z* plane. The majority of molecules in favorable scattering conditions correspond to confinement within the *y*, *z* plane.

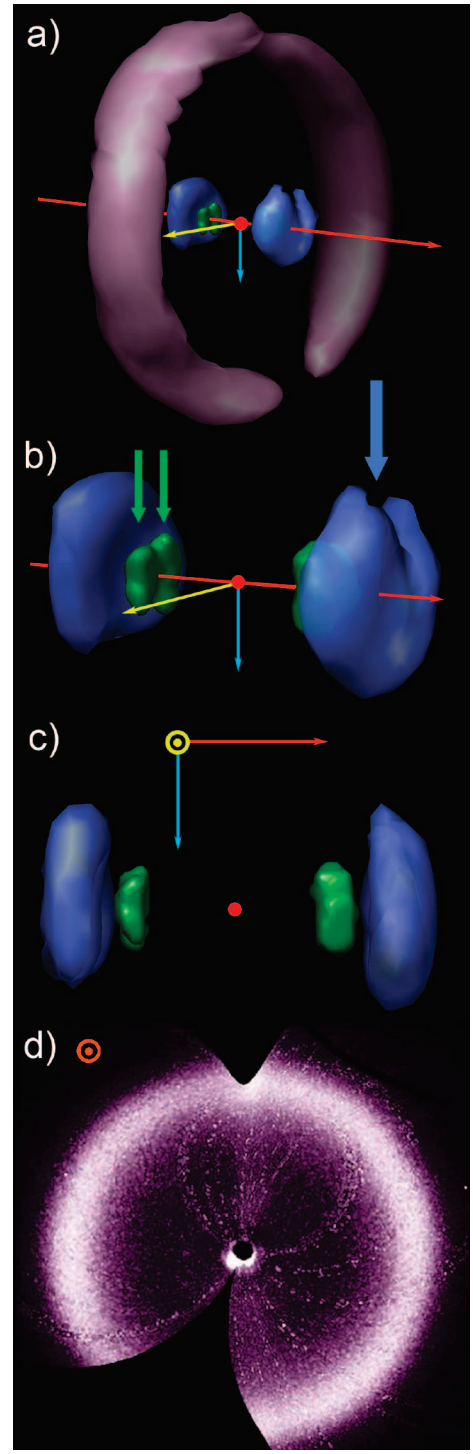

Figure 3. Three-dimensional diffraction of unstressed elastomer film. a) Data reconstruction minus the weak 14 Å feature. Radial components of the 38 Å (green) and 24 Å (blue) features have been expanded 2× relative to the 4.3 Å feature (purple). (b) Expanded view highlighting the splitting of the 38 Å feature (green arrows). The weak splitting associated with the 24 Å feature is also visible (blue arrow). (c) 3D view along the *y* axis (width of the film). (d) Diffraction image along the length of the film (*z* axis). Axis colors correspond to the colors of the coordinate system in Figure 1c.

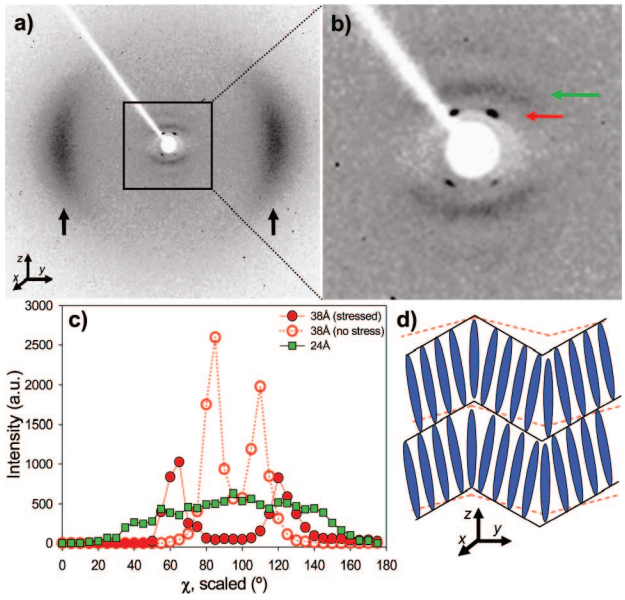

Figure 4. (a) Diffraction pattern of ELCE film under mechanical stress (~300 kPa). (b) Zoomed diffraction of layer information. The 38 Å splits into two distinct peaks and the 24 Å feature combines into a single wide band. Black, red, and green arrows correspond to 4.3, 38, and 24 Å diffraction features. (c) Intensity plotted as a function of χ for the 38 and 24 Å bands of the mechanically loaded sample. The unstressed 38 Å feature has been included for comparison (dotted line). (d) Schematic representation of chevron-like domain tilt in the absence of load (dashed red lines) and under tensile stress applied along the z axis (solid black lines).

In the 3D data, the wide angle band (4.3 Å) is consistent with features associated with the electroclinic liquid crystal packing within the layers and possesses cylindrical symmetry. When diffraction is viewed along the z axis, the diffuse ring (Figure 3d) indicates no observable preference or bias in the orientation of molecules parallel to the director (along the z axis). Although it is possible that there may be a small degeneracy around a cone angle of less than 20° or some slightly favored orientations along the z axis, it is not observed at the resolution of the 3D data.

Mechanical Loading. Panels a and b in Figure 4 display a diffraction image of the elastomer film with a tensile stress applied along the z axis. As the stress was increased, there was a distinct splitting of the 38 Å band into two well-separated spots and an accompanying increase in the χ separation angle between the two peaks. The split in the 38 Å band is the result of the expected chevron formation as the smectic layers within the film begin to buckle under mechanical load and has been observed previously in a smectic A elastomer subjected to mechanical stress.[15] In addition to the splitting, we observe about a 2-fold decrease in the overall intensity of the 38 Å band (Figure 4c). The intensity decrease implies a significant loss in the order of the smectic layers in favorable diffracting conditions. Such a decrease has been observed by Nishikawa and Finkelmann and was explained as a possible transition of the smectic elastomer into a nematic state as the load increased and the stress destroyed the layer ordering.[15] Adams and Warner suggested that a transition to a nematic state was unlikely and the decrease in intensity could rather be the result of polydomain formation in the elastomer.[9] In either case, only the layers with their normal confined in the y, z plane would diffract with a smectic elastomer under tensile stress, because all others would be rotated out of diffracting conditions. It is important to once again highlight the fact that our unstressed elastomer shows splitting of the 38 Å peak around the x axis a lack of rotational symmetry along the y axis in the 3D data. The 38 Å feature is split into two halves, the intensity of each half-being approximately the shape of a three-dimensional ellipsoid. It is possible that an increase in stress may destroy the preferred orientation, i.e., ellipsoidal shapes, of the 38 Å band and result in rotational symmetry about the z axis.

In addition to the changes in the 38 Å feature, it is of interest to note a subtle merger of the 24 Å band into a single broad peak (in contrast to the two weakly split peaks observed in the unstressed film). Integrating over the entire 24 Å band in the stressed elastomer reveals a minor decrease in the total intensity and a slight increase in the width of the band about χ compared to the unstressed elastomer. The same general trend of an intensity decrease and slight broadening of the band about χ also holds true for the faint 14 Å band. These collective observations imply that the layers in the observed diffraction plane are well-ordered, but there is an accompanying decrease in the number of domains in favorable scattering conditions upon application of a tensile stress. Additionally, the intermolecular packing and related intralayer features are maintained albeit with an associated reorientation.

E-Field Application. It is well-established that monomeric electroclinic systems show molecular tilt with an accompanying layer contraction. In addition, prior studies have shown that an ELCE will contract along the layer normal when subjected to an electric field.[3,11,12] Figure 5 displays two diffraction images of an elastomer film covered with gold foil electrodes and subjected to dc fields equal in magnitude (20 V/μm) but of opposite polarity. The applied fields caused several changes in the diffraction patterns, some of which were expected and others that provide novel insight into the details of the molecular switching mechanism of electroclinic elastomer films. As shown in Figure 5a, the maxima of the 4.3 Å band rotates clockwise about χ when a positive field is applied across the film, while switching to a negative polarity results in a counterclockwise rotation (Figure 5c). These expected observations reaffirm the electroclinic effect in our system because they correspond to coupling of the permanent electric dipole of the liquid crystal molecules to the applied field with a resulting molecular tilt. Analysis of the molecular rotation is shown in Figure 6a. There is a linear increase in the molecular tilt angle with increasing e-field strengths, which matches the 5° molecular tilt measured at the same field strengths using electro-optic techniques with polarized light microscopy.[3] It is clear that the direction, but not the magnitude, of the molecular rotation is dependent on the field polarity. The matching molecular tilt measured from X-ray scattering and electro-optic measurements suggests that the core region of the molecules has a strong contribution to the rotation of the 4.3 Å band (because electro-optic measurements are sensitive to changes in the core region of the molecule and are responsible for birefringence). The molecular tilt is accompanied by an

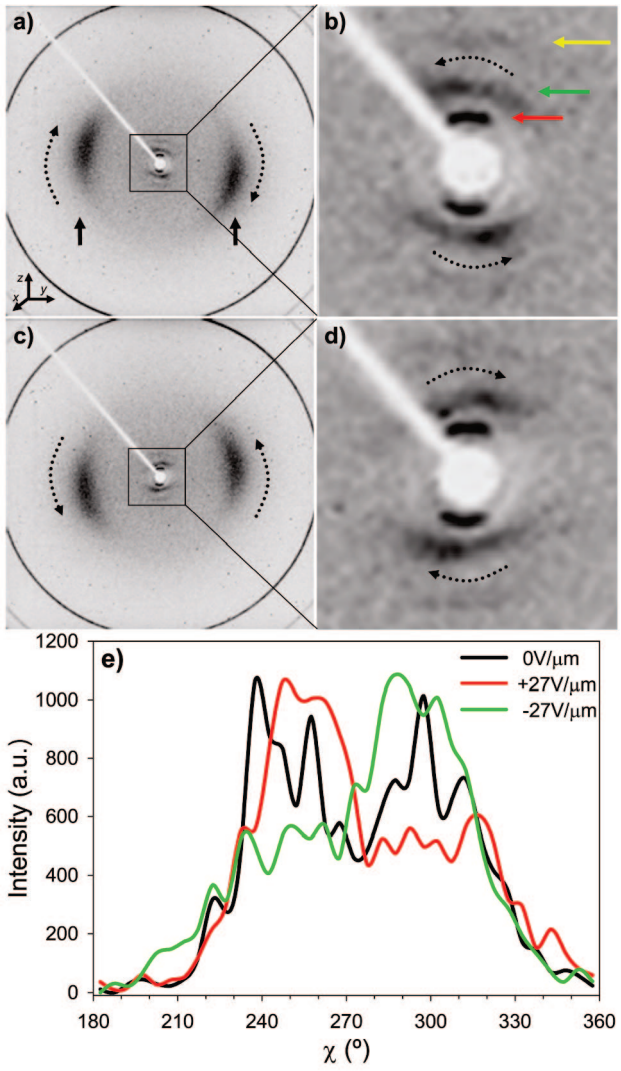

Figure 5. Diffraction of ELCE subjected to dc electric fields. (a) Diffraction pattern at +1600V displaying molecular tilting (curved arrows). (b) Zoomed in view showing shift in peak intensity of 24Å band (curved arrows). (c, d) represent the same field strength with opposite polarity. Diffraction rings in the image corners are scattering from the gold foil electrodes. Solid black, red, green, and yellow arrows correspond to 4.3, 38, 24, and 14 Å diffraction bands. (e) Plot of the integrated (and background subtracted) intensity of the 24 Å band vs χ for the sample subjected to 0 V (black), +27 V/μm (red), and −27 V/μm (green). The area under each curve reveals insignificant intensity differences (~3%) lower than the error associated with the signal-to-noise ratio.

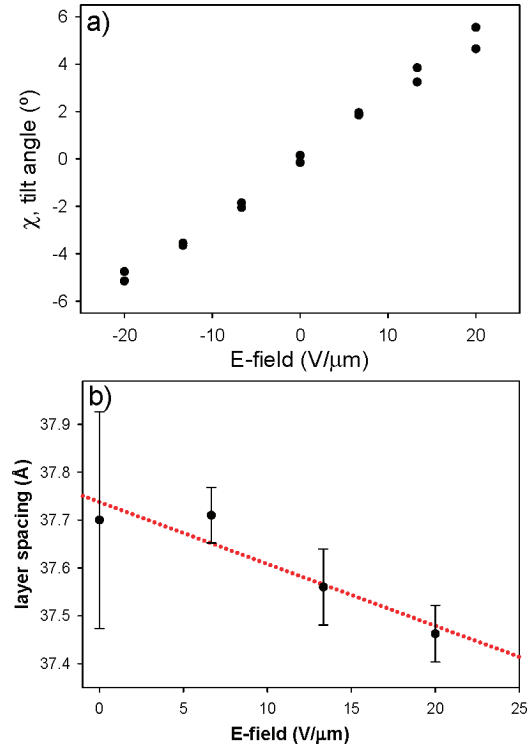

Figure 6. Effect of applied e-field on (a) the molecular rotation angle and (b) the layer spacing in an ELCE film.

expected layer contraction, i.e., a decrease in the *d*-spacing of the 38 Å band, with increasing electric field strength and, as expected, is independent of the field polarity (Figure 6b). Assuming the majority of the molecular switching is constrained to the *y*, *z* plane, the primary smectic layer spacing decreasing from 37.7 Å (0 V) to 37.5 Å (±20 V/μm) corresponds to a molecular tilt of ~6°. Taking into account the error associated with the detector resolution for the broad diffraction bands, these data are consistent with molecular tilting resulting in a decrease in the smectic layer spacing according to $\Delta l/l = 1 - \cos\theta$, where l is the primary smectic layer spacing and θ is the molecular tilt angle.

There is neither a detectable change in the intensity of the 38 Å band or a shift in the χ splitting of this band upon application of an e-field. This implies that there is no significant change in either the population of molecules in favorable diffracting conditions or in the orientation of the chevron-like domains when the X-ray beam is aligned with the *x* axis of the elastomer in the presence of an e-field. The same is not true for the 24 Å band, where a significant polarity-dependent rotation in the 24 Å peak intensity about χ is observed in a direction opposite to the rotation of the 4.3 Å band (compare panels a and b to panels c and d in Figure 5). It is important to note that the total intensity of the 24Å band in the unstressed state (0 V) or in the presence of e-fields of opposing polarity does not change significantly. Rather, it is only a change in the intensity distribution of the 24 Å band. As shown in Figure 5e, the intensity is distributed evenly between the two peaks in the 24 Å band in the unstressed state, whereas in the presence of an e-field, the intensity favors one of the peaks (Figure 5e). The shift in peak intensity without any accompanying decrease implies the redistribution of an intralayer feature into one of two preferred orientations when an e-field is applied. Given the molecular switching that follows the e-field, it is appropriate to assume that the intralayer feature corresponds to the rigid core of the molecule redistributing into a preferred orientation as the dipole aligns with the e-field. It should be noted that similar, but proportionately smaller, changes are seen at lower applied voltages for all the features described above.

There are no significant changes in the *d*-spacing of the 24 Å feature in the presence of an e-field. Likewise, there is no detectable change in the 14 Å band upon e-field application either in the *d*-spacing or the location of the peak intensity about χ, although this may be attributed to the difficulty in accurately measuring the peak location of this weak band. Finally, the main features of the 4.3 Å band, including the *d*-spacing and the total intensity, did not change significantly in the presence of an e-field. Taken together,

the diffraction features observed in the presence of an e-field imply that entire molecule (the acyl chain and rigid core) is tilting upon application of an e-field with no observable change in the intermolecular distance.

Discussion

Constructing a Model. The two-dimensional diffraction pattern imaged along the x axis (through the thickness) possesses three low-angle features with d-spacings of approximately 38, 24, and 14 Å. Previous attempts to explain the X-ray diffraction of layer-related information in smectic materials with a similar chemical composition index the maxima simply as $h = 1, 2, 3,...$ for a one-dimensional cell of repeat distance d.[18,19] However, this approach will fail when the periodicity is limited to a few cell repeats. Limited periodicity results in continuous scattering as a function of scattering angle with maxima not limited to the Bragg peak positions with integer values of h, an observation confirmed in the current two- and three-dimensional study. To address this key issue, we present a model based on periodic pair distribution functions. The model is consistent with the predominant features of the unstressed elastomer and accommodates the observed changes in the elastomer when subjected to either a tensile stress or an applied voltage. A theoretical diffraction pattern expressed as a function of a limited number of parameters is used to fit the experimental diffraction pattern. In light of the amount of scattering information available from the present studies, several different models may describe some of the features that have been observed experimentally. Although there is not sufficient independent data to establish the uniqueness of the PPDF-based model, it does provide the best description based on the diffraction data of the unstressed elastomer, particularly the 3D data, without being invalidated by the comprehensive collection of data of the film in either the presence of mechanical load or an e-field.

Smectic Layer Electron Density Profile. The near meridianal scattering related to the smectic layers appears to arise from two different orientations of a nearly one-dimensional structure, which is evidenced by the bifurcation observed in the unstressed elastomer (panels b and d in Figure 2). As shown in Figure 2c, integration of the intensity of the 38, 24, and 14 Å bands over χ is employed to obtain a one dimension diffraction pattern with the intent of obtaining a projection of the scattering density of a smectic layer onto the layer normal. As described in the Supporting Information, PPDFs are used to best match the electron density profile over a unit smectic layer. In so doing, the diffraction pattern is expressed as the sum of scattering arising from pairs of Gaussian scattering distributions within each elastomer layer and those in neighboring layers.

The first objective is to determine if the layer-related features belong to the same coherently scattering regions. Using the sum of intensities from 3 initial PPDFs, the model

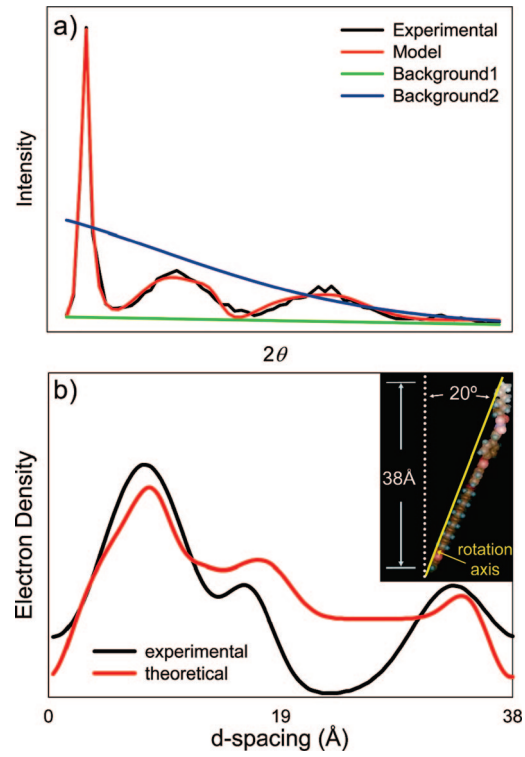

Figure 7. Modeling the experimental diffraction using PPDFs. (a) Experimental and model scattering comparison with background subtraction. (b) Experimentally (black) and theoretically (red) determined electron density profile of a unit smectic layer. Inset shows the energy-minimized electroclinic mesogen tilted 20° to fit layer spacing.

was able to fit experimental data reasonably well. One striking feature of this first attempt to model the layer-related information is that the sum of the two shorter distances equals the longest distance, which suggests that most of the scattering arises from two Gaussian regions within the same coherently scattered regions.

For M Gaussian distributions within each layer, the theoretical intensity may be expressed as the sum of $M(M - 1) + 1$ unique PPDFs. As a refinement to the initial theoretical fit and assuming that the layer information is indeed associated with a single phase, an intensity profile computed with PPDFs from three Gaussian regions is employed and fits the observed data very well, as shown in Figure 7a (red vs black curve). The sum of these three Gaussians is used to determine the projection of the electron density over a layer. The agreement factor, or R value, quantifies the discrepancy between the experimental data and theoretical fit and is defined as

$$R = \sum |I_{Ex} - I_{Th}| / \sum I_{Ex} \quad (1)$$

where I_{Ex} and I_{Th} are the experimental and theoretical intensities following background subtraction, respectively. The R value is calculated as 0.12, meaning the average deviation of the theoretical intensity from the experimental is only 12%. The background about which the PPDFs oscillate (Figure 7a, blue curve) is expressed as the sum of a straight line (Figure 7a, green curve) and a Gaussian function. Four parameters are varied in the refinement for the background, three for each Gaussian shaped scattering feature within a layer, and one for layer-to-layer variance,

(18) Artal, C.; Ros, M. B.; Serrano, J. L.; Pereda, N.; Etxebarria, J.; Folcia, C. L. *Macromolecules* **2001**, *34*, 4244.
(19) Omenat, A.; Hikmet, R. A. M.; Lub, J.; van der Sluis, P. *Macromolecules* **1996**, *29*, 6730.

for a total of 14 parameters. In order to fit the model to the experimental scattering information, the 11 best determined linear combinations of parameters that are eigenvectors of the least-squares equations are varied to produce a best fit.

In relating the electron density to the scattering features, it is clear that a single pair of infinitely sharp diffraction features with a 38 Å *d*-spacing indicates an infinitely periodic electron density with 38 Å between maxima. Deviations such as differences in the variance of the periodic pair functions that are correlated only over several nearest neighbor periods give rise to the broad maxima observed in the diffraction pattern at 24 and 14 Å. After several layers, the intralayer correlation diminishes to the point where the PPDFs yield a single broad feature (see the Supporting Information for more details).

Molecular Fit to Layer Spacing. On the basis of the experimental data alone, the precise boundary from one smectic layer to another cannot be determined. Therefore, it is necessary to incorporate a molecular model that best fits the electron density profile over a smectic layer in the electroclinic elastomer. The first step in deriving such a model is to fit the experimentally determined electron density projection with the energy-minimized liquid crystal molecular species in the elastomer. While energy minimization of single molecules may not represent the structural conformation of packed molecules within the elastomer, several favorable molecular conformations and a 70/30% ratio of the two main electroclinic components are considered in fitting the electron density profile. Given the resolution of the three low-angle features of the diffraction data (~10 Å), the important constraints and features of the model molecules are the overall length, the orientation of the NO_2 dipoles relative to the hydrocarbon chains, and corresponding relative positions of electron density concentration.

Assuming the molecules have a cylindrical distribution with the layers, we construct a model with a projected scattering power that closely resembles the experimental data. In order to fit the energy minimized molecules within the 38 Å layer spacing, they are tilted approximately 20° with respect to the layer normal (Figure 7b, inset). After applying the 20° tilt, the molecule is then rotated about a central axis defined by the two atoms in the molecule with the greatest separation parallel to the layer normal. In doing so, a molecular orientation is obtained for which the theoretical projection of the electron density agrees well with the experimental electron density (Figure 7b). It should be pointed out that the molecular tilt used to fit within the 38Å spacing is not confined to the *z*, *y* plane (Figure 8a), which is consistent with the experimental observations of a full width angular spread of ~45° at half-height for the molecular distribution when viewed along the *y* axis.

Unstressed Sample. Using the best-fit orientation of the liquid crystal molecules, the model is developed to be consistent with the diffraction from the unstressed material. To satisfy the width of the diffuse 4.3Å information, which indicates a relatively low number of adjacent molecules scattering coherently, and its orthogonal relation to the *z* axis, the model incorporates a small (<10°) molecular tilt confined to the *y*, *z* plane with no preferred orientation.

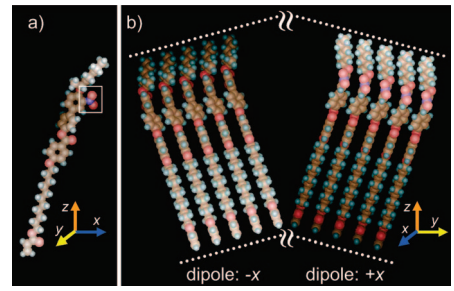

Figure 8. (a) Molecular model of ACN115 with proposed tilt that fits the electron density profile. The nitro dipole is indicated (white box). b) Molecular model displaying a single species (ACN115) arranged in two small chevron-like domains (dotted white lines) to qualitatively reproduce the predominant diffraction features of the experimental data. Nitro dipoles are oriented into the page ($-x$) and out of the page ($+x$) for the left and right chevron halves, respectively.

The χ splitting of the 24 Å peaks is greater than the splitting of the 38 Å peaks in an unstressed sample which suggests the two chevron-like domains have different preferred orientations for the permanent molecular NO_2 dipoles (Figure 8b). Incorporating NO_2 dipoles on one side of the chevron to be preferentially oriented opposite to the dipoles in the other side of the chevron into the model yields diffraction patterns that are qualitatively consistent with experimental observations. This holds true for not only the layer diffraction information, but also accounts for the fact that the combined distribution of the two orientations would result in the 4.3 Å diffraction information appearing nearly cylindrical when viewed along the *z* axis. If all of the features associated with each side of the chevron had the same χ splitting, this would indicate a true one-dimensional order in each side of the chevron corresponding to a conical distribution of molecular orientation generated by an axis of rotation normal to the layers, but this is not consistent with the diffraction data.

The two preferred dipole orientations in each of the chevron-like domains is a critical element in describing a model that on average represents the molecular packing in the electroclinic elastomer. While the model does not describe a 2-fold symmetry on the level of adjacent molecules, regions with different chevron-like domain orientations may be related by a 2-fold symmetry parallel the *z* axis. In addition, the model can also account for regions with the same chevron-like domain orientation related by a 2-fold symmetry parallel to the *x* axis. By accommodating such 2-fold symmetries within the elastomer, the model is able to qualitatively reproduce the experimental diffraction patterns. Within each half of a chevron-like domain, which may consist of 2−5 molecules, the intermolecular spacing is 4.3 Å and the NO_2 dipoles are oriented in opposite directions. As shown in Figure 8b, the normal of the stacked domains are rotated by 15° about the *x* axis to be consistent with the deviation of the chevron-like domains in the unstressed elastomer diffraction pattern. The finer details of the model diffraction are not expected to be present from the experimental data because of greater variance in the molecular orientation throughout the sample.

Two prominent features of the model are that neither the intermolecular spacing (4.3 Å information) nor the 24 Å

intralayer information lie perpendicular to the layer normal. The result is that the model captures an important and distinct feature of the experimental data, namely that from the chevron-like scattering, the χ separation of the 24 Å peaks is greater than that of the 38 Å peaks. In addition, because the model diffraction patterns were calculated on the basis of a grouping of a few liquid crystal molecules, the patterns correspond to scattering from within the smectic layers and assume that adjacent layers have a random lateral separation of such groupings. The 38 Å peak arises from the random lateral stacking of many adjacent layers and lies on the layer normal.

Mechanical Loading and E-field Application. The PPDF-based model is consistent with the observations in the presence of a tensile stress or an electrical field. However, it must be emphasized that observations in either of these two conditions are limited to a single diffraction plane (y, z) and, therefore, one can only speculate on the extent to which the model can describe and predict some of the more detailed features observed in either condition. Ultimately, the goal of capturing 3D data of the elastomer in the presence of either a tensile stress or an electric field test would first provide a complete picture of the elastomer realignment and further validate the PPDF-based model.

When a tensile stress is applied along the z axis, the chevron-like components rotate further away from one another with respect to the y-axis, reaching a maximum of $\sim$30° and increasing the split of the observed 38 Å peaks. In addition, the 38 Å bands sharpen to well-defined spots accompanied with a marked decrease in the intensity as the stress is increased and the 24 Å peaks merge into a single broadband with no significant change in the overall intensity. By increasing the deviation of the two chevron-like domains, the model can account for the observed increase in the splitting about χ as the tensile stress along z increases. The decrease in intensity of the primary layer diffraction information (located at 38 Å in the present study) has been observed previously in a SmA elastomer and has been interpreted as ordered blocks or regions of the elastomer rotating out of diffracting conditions, which would be consistent with our observations.[9,15] As the sample is stressed, some of the stacked layers rotate about the y axis such that the layer normal are no longer perpendicular to the X-ray beam and removed from favorable diffracting conditions. Those that remain in diffracting conditions are well-aligned in the presence of the mechanical field, resulting in defined spots. Because of the fact that data is collected with the X-ray beam aligned along the x axis, the model is limited in describing the changes associated with the 24 Å feature. To account for the unchanged total intensity associated with the 24 Å feature and the reduction from two peaks to a single broad peak, it appears that despite the 38 Å regions going out of diffracting conditions the shorter range features associated with the 24 Å peak persist. Tensile stress reduces the preferred domains of the 24 Å feature to a single broad distribution aligned with the z axis (and direction of the applied stress).

Diffraction data for the electrically actuated sample is also confined to the y, z plane, thus limiting the extent to which the model can be validated when subjected to an electric field. The split of the 38 Å band does not undergo a significant change in the presence of an e-field yet the maxima of the 24 and 4.3 Å features rotate in opposite directions about χ. The fact that there is not a significant intensity change in any of the diffraction features (there is only a redistribution of intensity) is a clear indication that the liquid crystal molecules are realigning in the presence of the e-field, a feature that the model can account for. It should be noted that despite the fact that an intensity redistribution is observed upon electrical actuation, molecules in their lowest energy orientations in the e-field need not be confined to orientations that produce the diffractions in the 24 and 14 Å regions for 2D data.

On the basis of the model and considering the observed diffraction changes, the 24 Å band may be decomposed into two scattering components, one associated with each of the chevron-like domains. Because there is no significant change in total intensity in the presence of an e-field, the area of each scattering component sharpens or broadens at a fixed χ value in accordance with the observed shifts in the 24 Å intensity. The change in the profile of each scattering component corresponds to a molecular reorientation. The exact nature of the reorientation cannot be deduced from the data set we have collected, but there are several speculative possibilities of molecular realignment that would be consistent with the model and also fit the e-field observations. The same decomposition of the 24 Å feature can be applied to the mechanically stressed material. In this case, the broadening of the two bands in the model can qualitatively predict merger of the two 24 Å peaks into a single broad peak. It is interesting to point out that, based on the PPDF model, we can associate an enhancement of 38 Å scattering component to a broadening of the 24 Å component.

One important observation to address is why the 4.3 and 24 Å features rotate in opposite directions about χ when the polarity of the electric field is switched. One possible explanation is that the preparation of the sample has produced two preferred domains throughout the elastomer in which the molecular dipoles are, on average, oriented opposite to one another. Application of a 0.5 Hz AC field when the monomeric liquid crystal mixture is being aligned may lend itself toward the creation of two preferred domains, despite the fact that the e-field is removed prior to the start of photopolymerization. The molecules in one domain predominantly have their dipoles aligned with one field polarity and vice versa. In the elastomer, application of an electric field would reorient many of the molecules, which are tethered to the polymer backbone, such that they tilt and rotate slightly and reduce the layer spacing. This accounts for the 4.3 Å band rotation about χ and the small reduction in the 38 Å band with respect to the solid cone angle, 2θ. The applied field and subsequent molecular rotation result in an enhancement of the scattering component of the 24 Å feature that corresponds with a now biased dipole alignment based on the field polarity, which is expected. Now, because of the presence of a single favored dipole orientation the number of molecules in scattering conditions in the other component is significantly reduced. Although this may not

be the absolute correct interpretation of the molecular reorientation, it is a plausible explanation and is consistent with the PPDF-based model.

Conclusion

For the first time, X-ray diffraction patterns have been collected of an electroclinic elastomer in three distinct states: unstressed, under mechanical load, and in the presence of e-fields of varying strength and polarity. The diffraction data reveals a non uniaxial molecular network with two preferred chevron-like domains associated with the smectic layers. Instead of simple indexing of layer-related maxima or interpreting the data as interdigitated smectic layers, PPDFs have been employed to satisfactorily describe the scattering data and suggests that the layer-related information belong to the same coherently scattering regions within the sample. Determination of the experimental electron scattering density over a unit smectic layer has allowed fitting of the liquid crystal molecular species and reveals a significant molecular tilt not confined to the y, z plane of the unstressed elastomer. The model can accommodate the changes observed in the elastomer when under mechanical stress or in the presence of an e-field. Although collection of a single plane of the 2D diffraction data for the stressed and actuated elastomers limits the ability to validate the uniqueness of the PPDF-based model, both the scattering data and the model provide valuable insight into the molecular packing and reorientation the electroclinic elastomer. More complex experimental setups will allow complete scattering data sets to be captured on the stressed and actuated sample and further reveal the molecular reorientations associated with this novel elastomer and provide opportunity for material improvements of this unique actuator material.

Acknowledgment. We thank the Office of Naval Research for funding support.

Supporting Information Available: Mathematical description and further detailed discussion of the periodic pair distribution functions and analysis used to model the diffraction data (PDF). This material is available free of charge via the Internet at http://pubs.acs.org.

CM801335J